

3D reconstruction of lungs from sparse thoracic CT images based on point cloud processing

Caixia Liu; Jiying Lang; Mingyong Pang*

***Corresponding Author: Mingyong Pang**

Institute of EduInfo Science and Engineering, Nanjing Normal Univeristy, Nanjing, China.

Email: panion@netease.com

Abstract

Computerized Tomography (CT) has become one of the most important lung disease diagnosis techniques. In order to visualize and quantitatively analyze 3D lung tissues from sparse thoracic CT slices, we present a novel 3D lung reconstruction algorithm based on a point cloud processing technology, which contains two principal stages: lung segmentation and lung reconstruction. In the first stage, we first segment lung CT images into a set of superpixels, and classify the superpixels using a random forest approach based on multi-scale features learned by a Convolutional Neural Network-Sparse Auto-Encoder (CNN-SAE) model. We then extract lungs from the classification result and further refine the segmented lungs with a set of post-processing techniques. In the second stage, we capture lung contours between adjacent lung segmentations from sparse slices with a gradient vector flow field snake model to construct 3D point cloud of lungs, and we finally constructed the 3D lungs with a floating scale surface reconstruction approach. Several experiments are conducted to test the performance of our algorithm, and the results shown that our algorithm can reconstruct lungs well from sparse lung CT slices, which can provide reliable information for effective observation and diagnosis of lung diseases.

Key words

Lung segmentation; Convolutional neural network; Superpixel; GVF; 3D Reconstruction.

Introduction

In many medical scientific and technical activities, Three-Dimensional (3D) organ models need to be reconstructed from serial two-dimensional (2D) medical slices, which is helpful for comprehending the structure of the organ and facilitating its automatic manipulation and analysis [1,2]. In recent years, 3D reconstruction of medical images has been widely used in medical teaching, human simulation, prosthetic and plastic surgery, virtual surgery, radiotherapy planning and so on.

3D reconstruction methods can be divided into two classes: surface rendering and volume rendering [3]. Surface rendering synthesizes surfaces by extracting points with the same gray value and building geometries including triangles, polygons, etc. Volume rendering projects a 3D data field onto 2D screen and synthesizes the model by calculating the values of pixels of the 2D projection image. Many researchers have proposed various 3D reconstruction algorithms of medical images. Yasaka et al. [4] reconstructed high-resolution computed tomography images using model-based iterative reconstruction and spatial resolution preference algorithm (MBIRn), conventional model-based iterative reconstruction and adaptive statistical iterative reconstruction for evaluating lung nodules, respectively. Xiao et al. [5] reconstructed a 3D model of lungs through several orthogonal scans using a compression sensing technique. Aiming to construct 3D surfaces from contours of axial slices, Mukundan et al. [6] proposed an algorithm for automatic segmentation of large volume sets and a contour-based construction of a 3D mesh representation. Hu et al. [7] proposed an improved marching cubes algorithm based on a universal tree structure and a contour points method for the 3D reconstruction of abdominal organ CT images. Zhang et al. [8] proposed a medical CT image reconstruction method with limited angle projection for incomplete scanning data set, which can satisfy the completeness condition of projection data. Guo et al. [9] implemented interpolation in 3D medical image reconstruction by a combined operation of weighted dilation and erosion. Zhu et al. [10] presented a brain reconstruction approach from magnetic resonance imaging (MRI) images based on domain-transform manifold learning. Huang et al. [11] proposed an algorithm for magnetic resonance (MR) image reconstruction, which minimized a linear combination of three terms corresponding to a least-squares data fitting, total variation (TV) and L1 norm regularization.

Active contour model has been widely used for capturing accurate contours of organs from medical images. Kim et al. [12] proposed a deformable model-based approach for vessel boundary detection and 3D reconstruction, where contours of vessels were obtained by Gradient Vector Field (GVF) Snake model [13] and then a 3D structure was reconstructed with the coordinates of the Snakes. In [14], edges were extracted using a multi-scale wavelet transform and refined with GVF Snake model. Then, combined with the shortest diagonal line method and the adjacent contours synchronous marching algorithm, a 3D surface reconstruction algorithm was proposed to reconstruct organ model from medical images. In order to capture accurate contours of organs from medical images for 3D reconstruction, Zhao et al. [15] proposed an improved watershed algorithm, which grew an organ in a CT image from a seed block by the principle of the similarity between grayscale and texture. Then they used the edge captured by the watershed algorithm as a start contour of the adjacent CT sequence, and segmented the organ from a sequence of images with GVF algorithm. Li et al. [16] presented a slice image-based 3D model reconstruction method. They extracted object outermost contours from slice images employing an improved GVF Snake model with an optimized force field and the ray method. And then they reconstructed a 3D model by contour connection using an improved shortest diagonal method and judgment function of contour fracture.

CT uses the X-ray, -ray, ultrasonic, and so on, together with a very sensitive detector around a thoracic part of the body one after another for cross-sectional scanning, and each of scanning forms a 2D lung image layer (slice). The main tasks in 3D reconstruction process of lung CT medical images usually include regions of interest (ROI) extraction from all the 2D layers and surfaces or volumes reconstruction of ROIs [17].

Although many available 3D reconstruction methods can be applied in 3D lung reconstruction of CT slices, there are still two challenging issues in them. First, in most cases, the target contour lines on the existing slices are first extracted with some techniques and refined with some edge extraction models such as GVF. Then a contour line connection methods [14,16] is adopted to reconstruct organ surface. However, this technical pipeline cannot deal with the inconsistently topologies of the upper and lower contours well [18]. For example, there are two closed contours in the upper CT slice while there is one contour in the lower CT slice. In this case, it is difficulty to determine the correct line connection between the two neighboring slices. Second, most of the current methods do not take sparse CT image reconstruction into account. Interslice distance refers to the distance between two successive image layers. If the interslice distance is small enough (<2 mm), the appearance of the 3D object can be recaptured simply by stacking up the ROIs in the correct order. However, if neighboring slices are not closely spaced (which we call sparse CT images), it is difficult to build an accurate 3D object from their 2D serial sections. Accordingly, capturing missing contours between contours of neighboring slices is of vital importance to reconstruct the appearance of 3D object [9].

In this paper, we proposed a novel 3D reconstruction algorithm. A convolutional neural network-stacked auto-encoder (CNN-SAE) model is used to extract accurate lung regions from CT slices and GVF snake model is employed to automatically capture the missing contours with convergences of the variable contour lines. Points on the contours are extracted and 3D image reconstruction approach based on the point cloud is utilized to reconstruct lungs. Our algorithm achieves lung reconstruction from sparse lung CT slices by transforming 2D sampling points into 3D spatial point cloud without considering the connection relation of the contour line itself.

The remainder of this paper is organized as follows: In Section \ref{sec:lungseg}, we present our lung segmentation algorithm and lung reconstruction algorithm, respectively. In Section \ref{sec:result}, we provide a set of experimental results and in Section \ref{sec:discussion}, we make a further discussion on the capabilities of our reconstruction framework and draw a brief conclusion in Section \ref{sec:conclusion}.

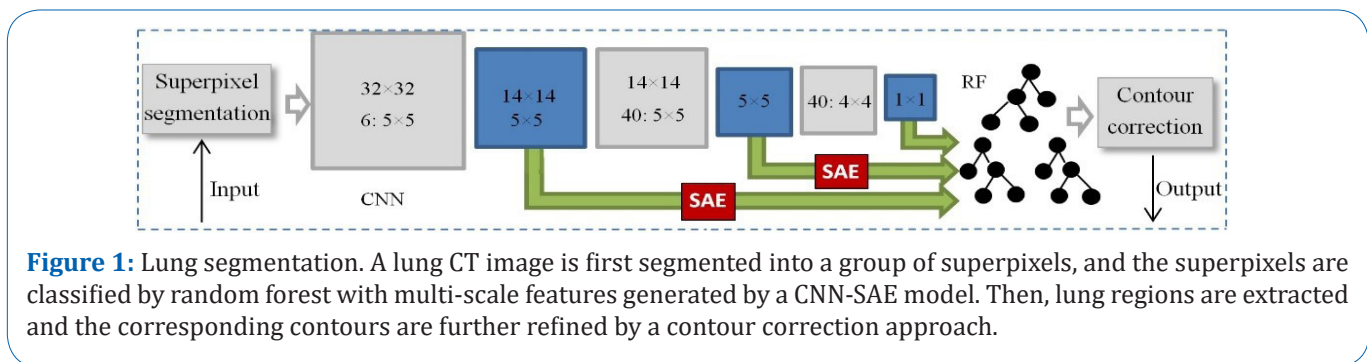
Methods

The images used in this paper come from the interstitial lung diseases (ILDs) dataset [19]. It contains High-Resolution Computed Tomography (HRCT) image series along with clinical parameters from patients with pathologically proven diagnoses of ILDs. The library contains 128 patients affected with one of 13 histological diagnoses of ILDs, 108 image series with more than 41 liters of annotated lung tissue patterns as well as a comprehensive set of 99 clinical parameters related to ILDs. Slice thickness is 1-2 mm, the spacing between two neighboring slices is 10-15 mm.

Lung segmentation

Accurate lung segmentation can provide more detailed contour information and is the base of accurate lung reconstruction. Our lung segmentation algorithm covers two stages: lung extraction and contour correction.

The input image is first segmented into a set of superpixels and then they are classified into four classes by Random Forest (RF) with multi-scale features of each superpixel captured from a Convolutional Neural Network-Sparse Autoencoder (CNN-SAE) model. Segmented lung contours are corrected with a corner detection-based technique. The pipeline of lung segmentation is shown in Figure 1.



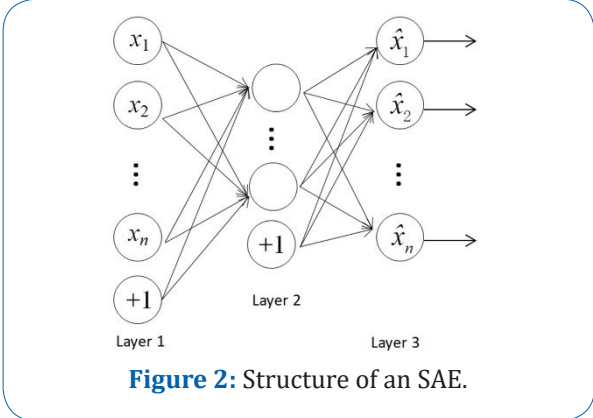
Lung segmentation with random forest based on multi-scale features

In lung segmentation, handcrafted features such as intensity, shape or texture cannot make representations of high-level problem domain concepts, which results in difficulty of characterizing certain classes efficiently [20]. Nevertheless, deep features are expected to be more powerful as they are learned from a massive amount of data in a supervised manner and are often more effective than traditional handcrafted features [21,22].

As we all know, CNN has the ability to represent learning, extracting and filtering input information layer by layer. The convolution layer of CNN can be regarded as a feature extractor, which generates local deep features of image patches in each layer, and finally combines these features into a global deep feature vector. In our model, deep convolutional features are extracted from lung CT images by a pre-trained deep network, CNN-SAE. The proposed CNN network is composed of six convolutional layers that have 6, 6 and 40 filters of size 5 x 5, 5 x 5 and 4 x 4, respectively. Each of the convolutional layers is followed by a max-pooling layer. The last pooling layer is connected to a fully-connected layer, which in turn, is connected to a softmax layer to calculate the output probability.

Auto-encoder is a type of feed-forward neural network, under the unsupervised setting, whose output is required to be equal to the input. SAE is a special three-layer neural network with a sparse limitation in general SAE and its structure is represented in Figure 2. The feature of SAE is that the node number of the input layer (Layer 1), excluding bias node, is the same as that of output layer (Layer 3), while the node number of the hidden layer (Layer 2) is less than that of the input layer and output layer nodes. SAE model used in our model is to obtain a low-dimensional representation of the original data. In the model, the node numbers of the input layer, hidden layer, and output layer are 25, 10 and 25, respectively. The activation function used in SAE is sigmoid with learning rate 1. Taking deep features of the first two convolutional layers as the input of SAE, combining the features extracted from the last convolutional layer of CNN, we obtain the multi-scale deep features of the input CT image after 100 iteration calculation.

A superpixel consists of a set of adjacent pixels with similar intensity, shape, texture, and other characteristics. It retains complete local information for further image segmentation [23]. In our algorithm, an input CT image is first segmented into a set of superpixels, and superpixel features extracted by the CNN-SAE model are taken as the input of a random forest classifier. Accordingly, the superpixels are classified into two classes: pleural tissues and other regions. The background of the CT image is extracted by a region growing approach and the superpixels in lung region are extracted by eliminating background using a group of morphological operations.



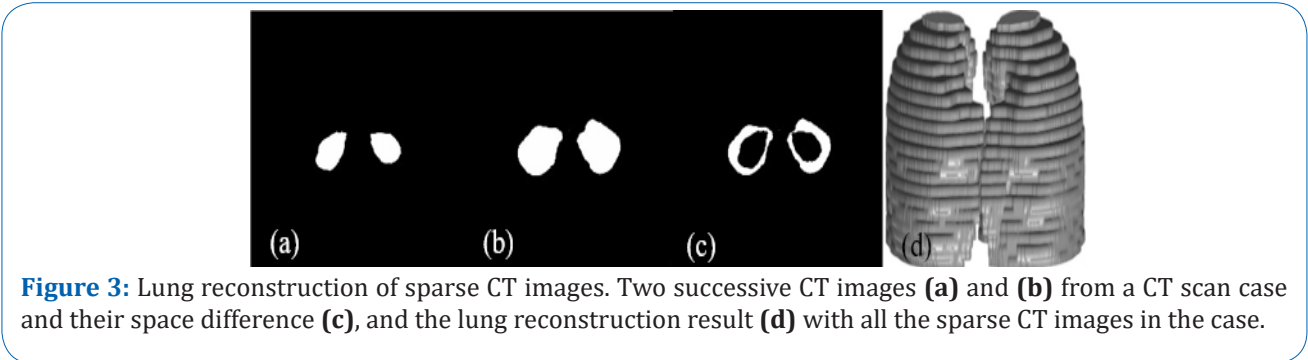
Contour correction

The lung contours segmented with our CNN-SAE model are usually incomplete because of lesions such as nodules and pneumonia. We use a contour correction approach based on a corner detection approach to refine our segmentation. The main steps are shown as:

- (1) Calculate corners on the lung contours with the Shi-Tomasi approach [24].
- (2) Adjacent corners are detected with a circle dilatation method [25] and connected with lines.
- (3) Smooth contours with a morphological closing operation and moving average method.

Lung reconstruction

As shown in Figure 3, if the interslice distances between successive slices are big (e.g. 10 mm in ILDs dataset), the appearance of the 3D object cannot be recaptured simply by stacking up the contours in the correct order (Figure 3d). In order to find the contours of slices locating at the space between two neighboring slices (Figure 3c), we utilize an active contour model, GVF, to automatically capture them.



Point cloud extraction

GVF Snake model [13] is derived from the traditional active snake model adding static external force field to expand the scope of the force field. The model can converge to concave areas of the object. Assume f is the edge map of a gray-scale image, and ∇f is the gradient field of f . f iteratively diffuses to edges of the image and forms gradient vector flow field for the image. Here we define gradient vector flow field as a vector field, and the new external force minimizes the energy function shown in Equation 1.

$$\begin{aligned} E &= \iint \mu \nabla^2 v + |\nabla f|^2 |v - \nabla f|^2 \, dx dy \\ &= \iint \mu (u_x^2 + u_y^2 + v_x^2 + v_y^2) + |\nabla f|^2 |v - \nabla f|^2 \, dx dy \end{aligned} \quad (1)$$

Where u_x, u_y, v_x and v_y are the first-order partial derivatives of u, v with respect to x and y , respectively. μ is a adjusting parameter, ∇^2 is the Laplace operator.

When the image gradient $|\nabla f|$ is relatively small, that is, when the dynamic curve is far from the real contours, the image energy is mainly dominated by the first term of Equation 1. On the other hand, when $|\nabla f|$ is relatively large, that is, when the dynamic curve is located on the contours or in its vicinity, the image energy is mainly dominated by the second term of Equation 1. The GVF field is expressed as Equation 2 according to Euler equation. The matching between the model and the target contour can be achieved by solving a minimum energy function $v = |\nabla f|$. To minimize the energy function, the gradient vector flow field satisfies the Euler equation expressed in Equation 2:

$$\begin{cases} u \nabla^2 u - (u - f_x)(f_x^2 + f_y^2) = 0 \\ u \nabla^2 v - (v - f_y)(f_x^2 + f_y^2) = 0 \end{cases} \quad (2)$$

Its iterative equation is

$$\begin{cases} u = u + \mu \nabla^2 v - (u - f_x)(f_x^2 + f_y^2) \\ v = v + \mu \nabla^2 u - (v - f_y)(f_x^2 + f_y^2) \end{cases} \quad (3)$$

And the iterative formula of contour convergence is:

$$\begin{cases} x = inv \times (\gamma \times x + \kappa \times \mu) \\ y = inv \times (\gamma \times y + \kappa \times \mu) \end{cases} \quad (4)$$

In GVF, $v(x, y)$ always points toward the edges with minimum energy. The initial contour moves to the real edge under the action of $v(x, y)$, and stops when the total energy of the contour reaches the minimum value, and the resulted contour is the real contour. The distance, d , at which the initial contour converges each time influences the rate of convergence. As shown in Figure 4, the contour in the next slice is taken as the initial contour of the current slice in a CT scan case. With the convergence of the initial contour, we obtain the evenly distributed contours, C'_s , between two neighboring slices (Figure 4). The number (density) of C'_s, C_n , is determined by convergence step, d , the smaller d in GVF algorithm generates bigger C_n as shown in Figure 5}. In our method, we set $d = 1$.

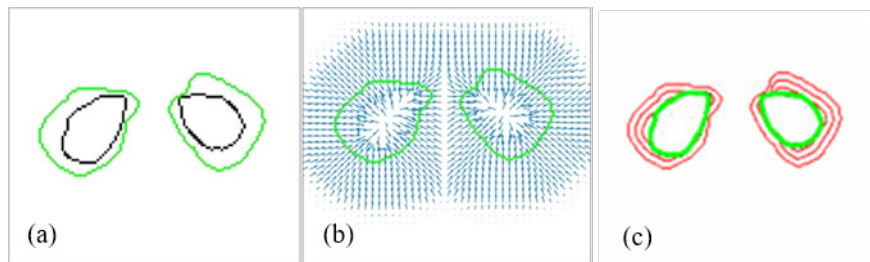


Figure 4: Capturing contour with GVF snake model. We set initial contours (green lines) in a upper slice using contours of its lower slice **(a)**. In gradient vector flow field **(b)**, initial contours convergence and form a set of intermediate contours between contours in two two adjacent slices **(c)**.

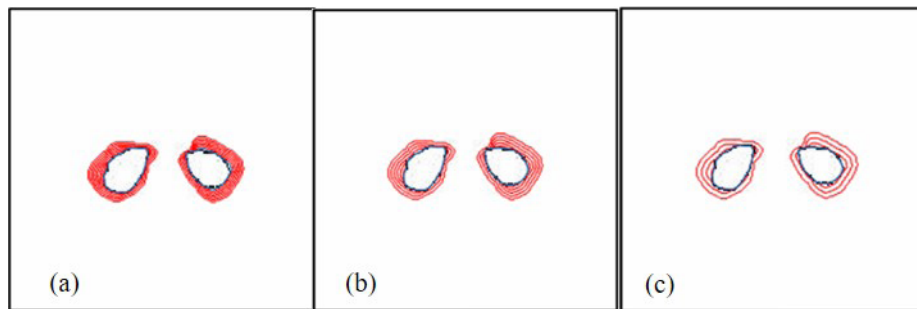


Figure 5: Different number (density) of C_n with various d_s , $d = 2$ (a), $d = 3$ (b), $d = 5$ (c).

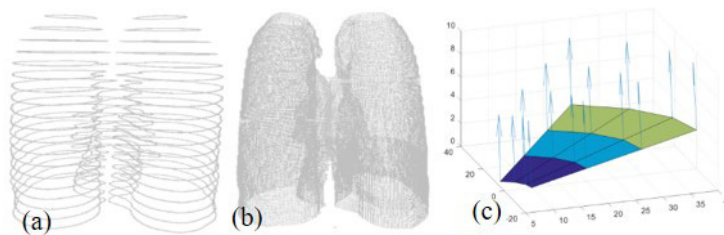


Figure 6: Point cloud. From existing sparse contours **(a)**, dense contours **(b)** can be generated through our method, which is helpful for calculating accurate point normals **(c)**.

With the points located on contours captured with our GVF model, we obtain the contour point cloud from a CT scan case (Figure 6b). Compared with the point cloud extracted from the original lung segmentation results (Figure 6a), our method can generate more contour points, which contributes to the point cloud reconstruction of lungs. For example, it is easily to calculate point normals according to the locally fitted surface of the region where the point is located.

Floating scale surface reconstruction

Compared with millions of sampling points in a general point cloud reconstruction model, there are about 40 thousand data points of each lung. Here, we employed Floating Scale Surface Reconstruction (FSSR) method for our reconstruction [26].

FSSR method can efficiently reconstruct high-quality meshes from acquired sample data. It reconstructs a real object surface by constructing an implicit function as the sum of compactly supported basis functions, and the implicit function has a continuous "floating" scale in space, which makes it a nearly parameter-free method. At the same time, it can correctly reconstruct a surface from sparse sample points.

FSSR covers three parts: building octree, calculating implicit function and extracting isosurface. First, we calculate the scale and normal vector of all the input sampling points [27,28]. Then all the sampled points are inserted into the octree data structure according to their scales. The eight corners of the octree leaf node are called voxels, where the implicit function values are calculated. Finally, the isosurface is extracted from the octree by using the variant of the marching cube algorithm [29]. The main steps are shown as follows:

1. Octree generation

Assume that a sample point i has scale value s_i and the radius is $3s_i$ according to the calculation of basic function defined as Eq.(5).

$$f(x_i) = f_x(x)f_y(x)f_z(x) = \frac{x}{\sigma^4 2\pi} e^{\frac{-1}{2\sigma^2}(x^2+y^2+z^2)} \quad (5)$$

Where $f_x(x) = \frac{x}{\sigma^2} e^{\frac{-x^2}{2\sigma^2}}$, $f_y(x) = f_z(x) = \frac{x}{\sigma\sqrt{2\pi}} e^{\frac{-x^2}{2\sigma^2}}$

Let the side length of an space octree node at level u_x is set u_y , we impose

$$S_l \leq s_i < S_{l-1} \Leftrightarrow S_l \leq s_i < 2S_l \quad (6)$$

when a sample point u_x is inserted into an octree node with a side edge length of u_y , the edge length is at most v_x :

$$\frac{1}{2}s_i < S_l \leq s_i \quad (5)$$

Starting from an empty octree, the first sample point i is inserted into a newly created root node with a central position, p_i . and a side edge length of s_i . We insert the subsequent sampled point according to the following steps:

(a) If the sampled point is outside the octree, the octree is iteratively expanded in the direction of the new sample until the new sample is inside the octree. Then we insert the sampled point according to (b) or (c).

(b) If the scale of the new sampled point is larger than the side length of the root node, the octree will continue to expand to generate a new and larger root node until the side length of the root node meets the Equation (6).

(c) If the scale of the new sampled point is smaller than the side length of the root node, the octree will be traversed. In this process, new nodes may be generated until the side length of a node satisfies the Equation (6).

Once the node location is determined, the sampled point is inserted into the tree.

(2) Implicit function evaluation

Suppose there is an input point set with N sampled points, and each of the point contains posi-

tion p_i , normal vector n_i and scale s_i . Variable scale reconstruction establishes a symbolic implicit function, which is positive or negative in or out of the implicit surface. The implicit function is defined as the weighted sum of the base function:

$$F(x) = \frac{\sum_i w_i(x) f_i(x)}{\sum_i W_i(x)} \quad (6)$$

Where $W(x) = \sum_i w_i(x)$ and w is weighting function. It is composed of asymmetric components in the x direction, and a rotation invariant component in y - and z - direction.

A series of voxels are generated by traversing the eight corners of each leaf node in assisting octree. Implicit functions are calculated in these voxel locations, and each voxel is identified by a unique ID to avoid the repetitive computation. In order to calculate the function value of voxel x quickly, an efficient query is designed in the octree and only the sampling points that probably affect the x value is selected: recursively query the octree nodes, and check whether they affect the y value or not. According to Equation 6, the maximum scale of sampling points in node N with side length S_N is $2S_N$. If node N contains sampling points affecting x , it needs to meet the following requirements:

$$\|x - center(N)\| - \sqrt{3} \frac{S_N}{2} > 3 \cdot 2S_N \quad (7)$$

Left hand side of the inequality is the nearest distance from the sampling point in N node to x , and right hand side is the maximum influence distance of the sampling point in N node. If the inequality holds, the node and its children nodes are skipped. Otherwise, check whether all the sampled points in the node meet the requirements, $|x - p_i| < 3s_i$, which can affect x . Find all sampling points that can affect the value of x , and calculate the value of x function according to Equation 8:

$$x_i = R_i \cdot (x - p_i) \quad (8)$$

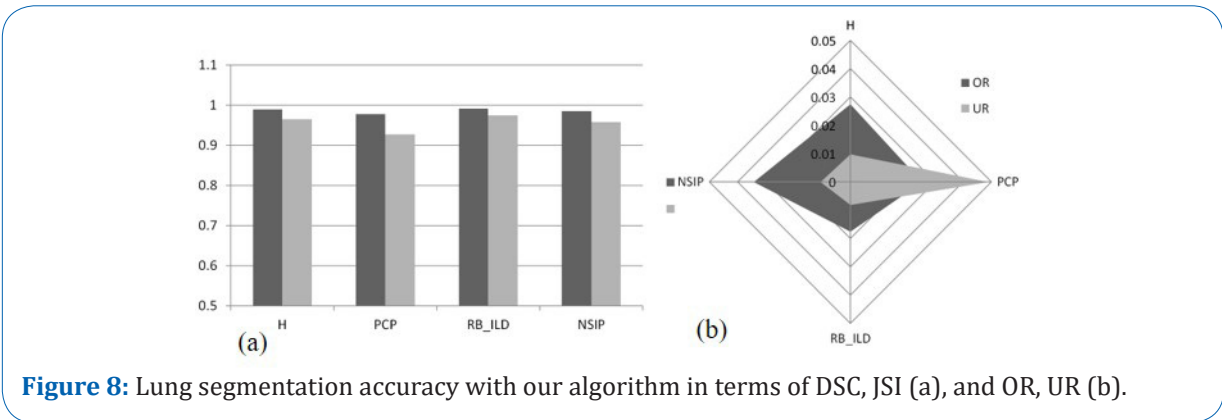
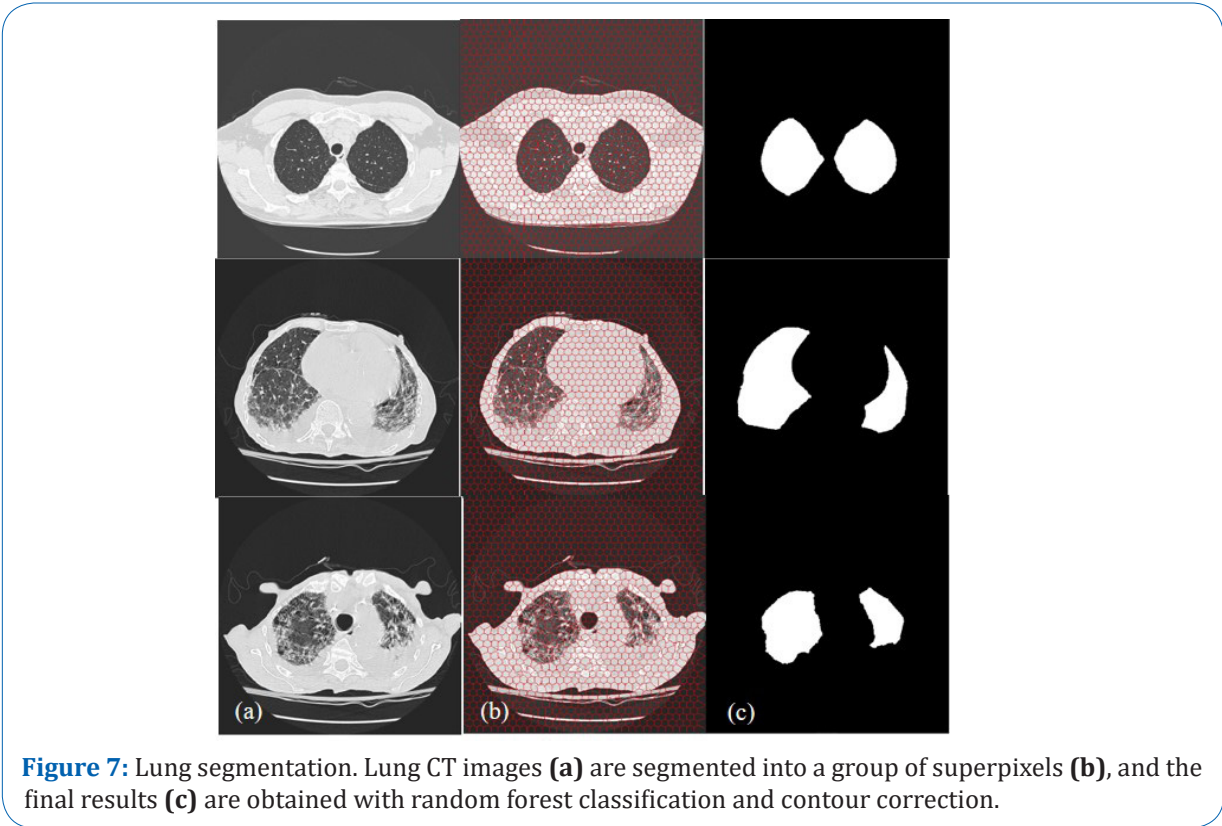
The rotation matrix $R_i = R(n_i)$ transforms voxel x into the local coordinate system (LCS) of sampled point i . LCS takes p_i as its original center and n_i is positive x -axis direction.

(3) Extract isosurface

Extract isosurface from the implicit function defined by the octree voxels. In general, each cube can be processed individually using the marching cubes [29], and the result mesh surface can be guaranteed to be watertight. However, because of depth disparity in the octree, and the common surface belonging to different cubes may make different judgments, which will leave cracks in the surface. Therefore, using a variant of the marching cube algorithm [29] can directly produce a non-cracked and highly adaptive grid from the octree hierarchy. After isosurface extraction [30] and color reconstruction, we obtain the reconstructed lungs.

Results

Accurate lung segmentation is helpful for the accurate lung reconstruction. We test the accuracy of our lung segmentation algorithm on an experimental data set including healthy (H), Pneumocystis Pneumonia (PCP), respiratory bronchiolitis associated ILD (RB\ILD) and nonspecific interstitial pneumonia (NSIP)CT images. Four classical metrics [25], Dice Similarity Coefficient (DSC), Jaccard's similarity index (JSI), over-segmentation rate (OR), under-segmentation rate (UR) is used for evaluating the performance of our lung segmentation algorithm. We show a group of lung segmentation results in Figure 7 and exhibit the corresponding segmentation accuracy in terms of DSC, JSI, OR and UR in Figure 8. It can be seen that the accuracy of PCP image segmentation is lower than other types of images due to their inhomogeneous intensities. Nevertheless, lung segmentation accuracy on all of the types of images is higher than 90% in terms of DSC and JSI, and lower than 0.05 in terms of OR and UR. Our algorithm can generate accurate lung segmentation, which is helpful for extracting correct point cloud for the lung reconstruction.



With point cloud extracted from lung contours, a set of reconstruction results of lungs using the FSSR algorithm. FSSR calculates the scale according to the spacing of sampled points, and the scale of sampling points is estimated by the average distance of k nearest neighbors. The reconstruction results are different with different k as shown in Figure 9. Smaller k generates coarse reconstruction results while bigger k produces more accurate results. However, some details will be smoothed if k is too big. Here, we empirically set $k=200$.

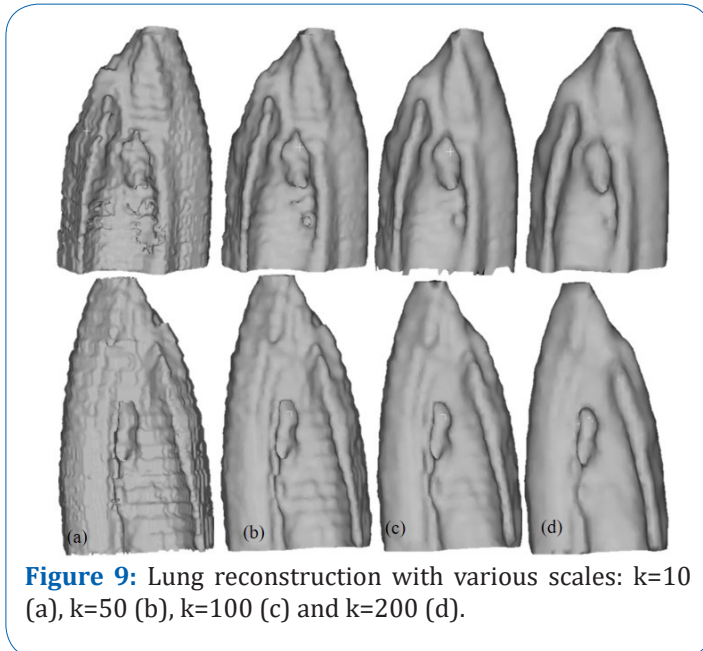


Figure 9: Lung reconstruction with various scales: $k=10$ (a), $k=50$ (b), $k=100$ (c) and $k=200$ (d).

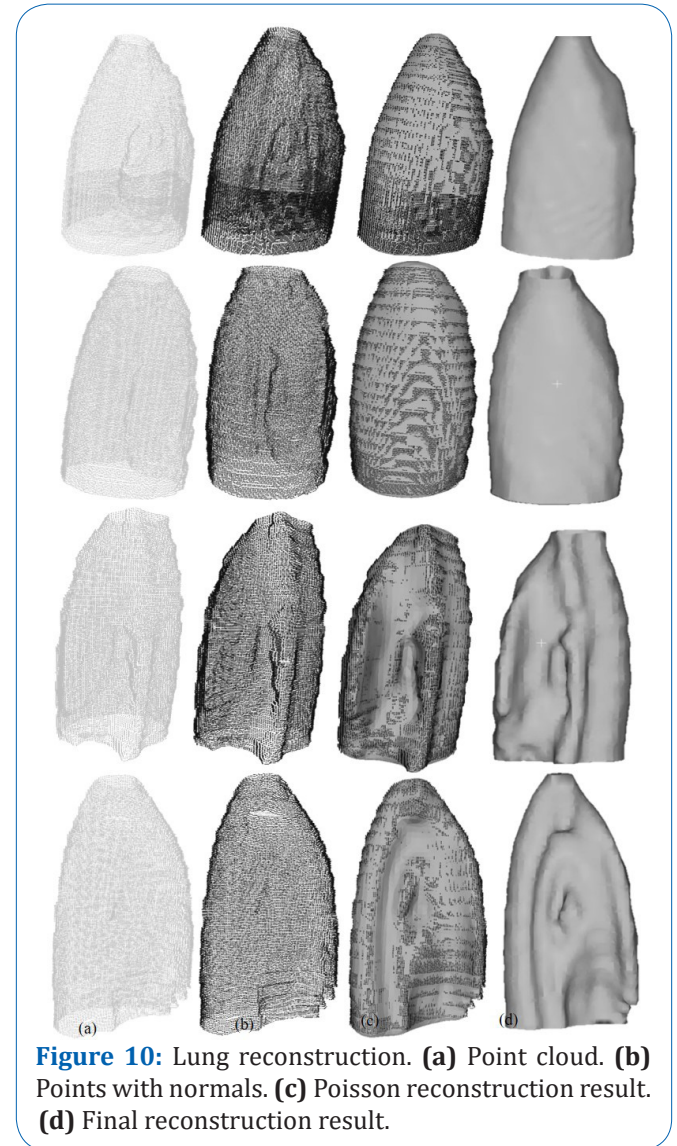


Figure 10: Lung reconstruction. (a) Point cloud. (b) Points with normals. (c) Poisson reconstruction result. (d) Final reconstruction result.

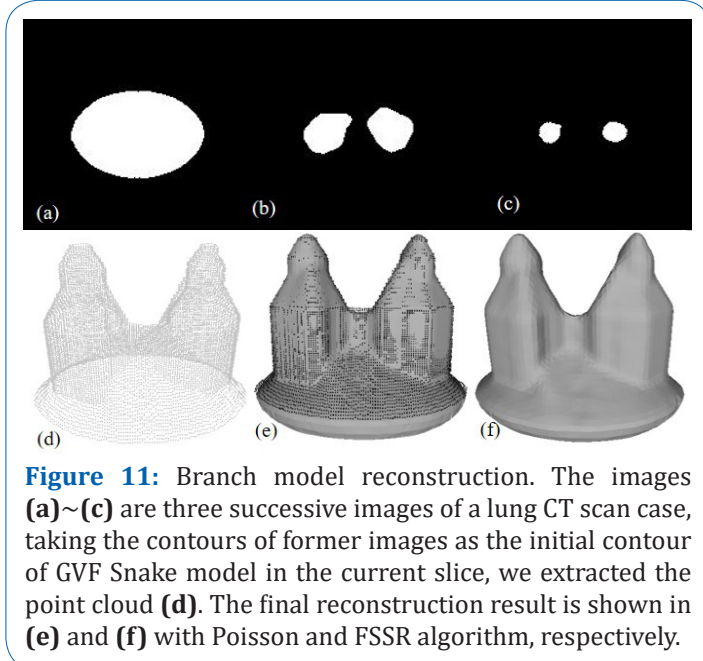


Figure 11: Branch model reconstruction. The images (a)~(c) are three successive images of a lung CT scan case, taking the contours of former images as the initial contour of GVF Snake model in the current slice, we extracted the point cloud (d). The final reconstruction result is shown in (e) and (f) with Poisson and FSSR algorithm, respectively.

Conclusion

3D lung reconstruction is to reconstruct 3D lung model from 2D medical image sequence, which is of great significance to medical anatomy, medical teaching clinical practice and so on. Compared with 2D CT images, 3D reconstruction of lungs can provide the observer with more intuitive, comprehensive and accurate information of lesions and normal tissues. In this paper, we introduce a novel 3D lung reconstruction

tion technique based on point cloud. We first use RF to distinguish accurate lung regions from the sparse lung CT images based on multi-scale features extracted with our CNN-SAE model. Then we use GVF Snake model to interpolate the missing contours, and obtain 3D point cloud of lung surface according to contour coordinates. Finally, we successfully reconstructed lungs with FSSR method. Our algorithm can deal with lung reconstruction from sparse lung CT images and can solve one-to-many contour matching problem, but for many-to-many contour matching problem, we need to further improve the contour interpolation algorithm to get more accurate reconstruction.

Acknowledgements: The work was supported by grants from the National Natural Science Foundation of China [No.62007028, 41631175, 61702068], the Key Project of Ministry of Education for the 13th 5-years Plan of National Education Science of China [No.DCA170302], the Social Science Foundation of Jiangsu Province of China [No.15TQB005], and the Priority Academic Program Development of Jiangsu Higher Education Institutions [No.1643320H111].

References

1. Lin WC, Liang CC. Dynamic elastic interpolation for 3D medical image reconstruction from serial cross sections. *IEEE Transactions on Medical Imaging*. 1988; 7: 225-232.
2. Guo JF, Cai YF, Wang YP. Morphology-based interpolation for 3D medical image reconstruction. *Computerized Medical Imaging and Graphics*. 1995; 19: 267-279.
3. Li MY, Wang B, Liu C. 3D reconstruction of CT image based on MC-E algorithm. *Computer Engineering and Design*. 2019; 40: 2959-2963.
4. Yasaka K, Katsura M, Hanaoka S, Sato J, Ohtomo K. High-resolution CT with new model-based iterative reconstruction with resolution preference algorithm in evaluations of lung nodules: Comparison with conventional model-based iterative reconstruction and adaptive statistical iterative reconstruction. *European Journal of Radiology*. 2016; 85: 599-606.
5. Xiao S, Lv Z, Xin Z. A lung 3D model reconstruction method based on compressed sensing and MRI. 2015 IET International Conference on Biomedical Image and Signal Processing (ICBISP 2015). 2016; 1-4.
6. Mukundan R. Reconstruction of High Resolution 3D Meshes of Lung Geometry from HRCT Contours. *IEEE International Symposium on Multimedia IEEE*. 2017; 247-252.
7. Hu LY, Shi K, Xu S. Improved marching cubes algorithm for 3D reconstruction. *Chin J Med Imaging Technol*. 2019; 35: 925-929.
8. Zhang J, Teng J, Bai Y. Improving Sparse Compressed Sensing Medical CT Image Reconstruction. *Automatic Control and Computer Sciences*. 2019; 53: 281-289.
9. Guo JF, Cai YL, Wang YP. Morphology-based interpolation for 3D medical image reconstruction. *Computerized Medical Imaging and Graphics*. 1995; 19: 267-279.
10. Zhu B, Liu J, Cauley SF, Rosen BR, Rosen MS. Image reconstruction by domain-transform manifold learning. *Nature*. 2018; 555: 487-492.
11. Huang J, Zhang S, Metaxas D. Efficient MR image reconstruction for compressed MR imaging. *Medical Image Analysis*. 2011; 15: 670-679.
12. Kim H, Ahn C, Jeong G. Vessel Boundary Detection for its 3D Reconstruction by Using a Deformable Model (GVF Snake). *IEEE Engineering in Medicine and Biology 27th Annual Conference*. Shanghai, China. 2006; 3440-3443.
13. Xu C, Prince JL. Gradient Vector Flow: A New External Force for Snakes. *IEEE Computer Society Conference on Computer Vision & Pattern Recognition*. 1997; 97: 66-71.

14. Cheng J, Liu Y, Bai L. 3D reconstruction from medical images with improved GVF snake model. International Conference on Computational Intelligence and Security, Suzhou, China. 2008; 220-224.
15. Zhao J, Yi FL, Huang ZP. A New Contour Initialization of CT Image Sequences in GVF Model. Applied Mechanics & Materials. 2013; 1225-1229.
16. Li HA, Kang BS. A 3D Model Reconstruction Method Using Slice Images. Computer Aided Drafting, Design and Manufacturing. 2013; 3: 5.
17. Chen SY, Lin WC. Improvement on dynamic elastic interpolation technique for reconstructing 3-D objects from serial cross sections [biomedical application]. IEEE Transactions on Medical Imaging. 1990; 9: 71.
18. Liu Y, Su Z. Complex surface reconstruction from biological image. Computer Engineering and Applications. 2011; 47: 18-21.
19. Depeursinge A, Vargas A, Platon A, Geissbuhler A, Poletti PA, et al. Building a reference multimedia database for interstitial lung diseases. Comput Med Imaging Graph. 2012; 36: 227-238.
20. Lai ZF, Deng HF. Medical Image Classification Based on Deep Features Extracted by Deep Model and Statistic Feature Fusion with Multilayer Perceptron. Computational Intelligence and Neuroscience. 2018; 1-13.
21. Babenko A, Lempitsky V. Aggregating Deep Convolutional Features for Image Retrieval. Computer Science. 2015; 1269-1277.
22. Li G, Yu Y. Visual Saliency Based on Multiscale Deep Features. Proceedings of the IEEE Conference on Computer Vision and Pattern Recognition. Boston, MA, USA. 2015; 5455-5463.
23. Achanta R, Shaji A, Smith K, Lucchi A, Fua P, et al. SLIC Superpixels Compared to State-of-the-Art Superpixel Methods. IEEE Transactions on Pattern Analysis & Machine Intelligence. 2012; 3: 42274-2282.
24. Tomasi JSC. Good Features To Track." Proc. IEEE Conf. Comput. Vision Pattern Recognit volume. 2002; 84: 593-600.
25. Liu C, Zhao R, Pang M. Lung segmentation based on random forest and multi-scale edge detection. IET Image Processing. 2019; 13: 1745-1754.
26. Fuhrmann S, Goesele M. Floating Scale Surface Reconstruction." ACM Transactions on Graphics. 2014; 33: 46-56.
27. Hoppe H. Surface reconstruction from unorganized points. ACM SIGGRAPH Computer Graphics. 1992; 26: 71-78.
28. Dey TK, Li G, Sun J. Normal estimation for point clouds: a comparison study for a Voronoi based method. Eurographics/IEEE Vgtc Symposium Point-based Graphics. 2005; 39-46.
29. Kazhdan M, Klein A, Dalal K. Unconstrained isosurface extraction on arbitrary octrees. Proceedings of the Fifth Eurographics Symposium on Geometry processing, Barcelona, Spain, 2007; 125-133.
30. Kazhdan MM, Bolitho M, Hoppe H. Screened Poisson Surface Reconstruction. Proceedings of the Fourth Eurographics Symposium on Geometry Processing, Cagliari, Sardinia, Italy, 2006.

Manuscript Information: Received: November 24, 2022; Accepted: January 02, 2023; Published: January 10, 2023

Authors Information: Caixia Liu¹; Jiying Lang²; Mingyong Pang^{2*}

¹College of Intelligent Education, Jiangsu Normal University, Xuzhou, China.

²Institute of EduInfo Science and Engineering, Nanjing Normal University, Nanjing, China.

Citation: Liu C, Lang J, Pang M. 3D reconstruction of lungs from sparse thoracic CT images based on point cloud processing. Open J Clin Med Case Rep. 2023; 1960.

Copy right statement: Content published in the journal follows Creative Commons Attribution License (<http://creativecommons.org/licenses/by/4.0>). © **Pang M (2023)**.

About the Journal: Open Journal of Clinical and Medical Case Reports is an international, open access, peer reviewed Journal focusing exclusively on case reports covering all areas of clinical & medical sciences.

Visit the journal website at www.jclinmedcasereports.com

For reprints and other information, contact info@jclinmedcasereports.com